Journal of Solid State Chemistry **145,** 104–109 (1999)
Article ID jssc.1999.8228, available online at http://www.idealibrary.com on IDEAL®

Magnetic Properties of $Ba_{1-x}La_xPrO_3$ and $PrLu_{1-y}Mg_yO_3$ with x and $y \leq 0.075$

Masahiro Itoh, Keitaro Tezuka, Makoto Wakeshima, and Yukio Hinatsu

Division of Chemistry, Graduate School of Science, Hokkaido University, Sapporo 060-0810, Japan

Received November 12, 1998; in revised form February 5, 1999; accepted February 15, 1999

The perovskite-type $Ba_{1-x}La_xPrO_3$ ($0 \leq x \leq 0.15$) and $PrLu_{1-y}Mg_yO_3$($0 \leq y \leq 0.20$) solid solutions containing mixed valent praseodymium ions were prepared. Their powder X-ray diffraction measurements were carried out and the magnetic susceptibilities were measured in the temperature range between 4.2 and 300 K. The compound $PrLuO_3$ was prepared for the first time in this study and its crystal structure has been determined to be an orthorhombically distorted perovskite with space group *Pnma*. From their magnetic susceptibilities, it was observed that magnetic exchange interactions between Pr ions in the $Ba_{1-x}La_xPrO_3$ solid solutions were weakened with the La^{3+} substitution for the Ba^{2+}. $PrLu_{1-y}Mg_yO_3$ has no magnetic ordering down to 4.2 K. The difference in magnetic properties of praseodymium ions between at the *A*-site and at the *B*-site of the perovskite structure ABO_3 was discussed. © 1999 Academic Press

INTRODUCTION

The most stable oxidation state of rare earth elements are trivalent. In addition to this state, cerium, praseodymium, and terbium have the tetravalent state (1). We are interested in the electronic state of tetravalent praseodymium ions in solids. The electron configuration of Pr^{4+} ion is $[Xe]4f^1$ ([Xe], xenon electronic core) which makes its electronic analysis straightforward. Perovskite type oxides, ABO_3, where A is a divalent ion (e.g., Sr, Ba), accommodate tetravalent metal ions at the B site of the crystal. The B site ions sit at the center of the octahedron formed by six oxygen ions.

The perovskite compound $BaPrO_3$ in which the oxidation state of the praseodymium ion is tetravalent shows various anomalous magnetic properties. This compound shows an antiferromagnetic transition at 11.6 K and a very sharp drop in the susceptibility is observed when the temperature is increased through this transition temperature (2). This magnetic ordering corresponds to the λ-type anomaly found in the heat capacity vs temperature curve (3). Some magnetic susceptibility measurements reported that a weak ferromagnetic-like behavior was observed in the antiferromagnetic component (4, 5) and recent high-resolution neutron powder diffraction shows that the Pr spins are staggered along the c-axis with an averaged moment of 0.35 μ_B (6). Even in the paramagnetic region, the Pr ion in the $BaPrO_3$ shows an interesting behavior: a large temperature -independent paramagnetic susceptibility ($\chi_{TIP} = 6.4 \times 10^{-4}$ emu/mole) and a small effective magnetic moment ($\mu_{eff} = 0.68\ \mu_B$) (7). In our previous study, $Ba_{1-y}Sr_yPrO_3$ ($0 \leq y \leq 1$)solid solutions were prepared, and through their magnetic susceptibility measurements, the magnetic interactions between Pr^{4+} ions were found to be weakened when substituting a strontium atom for the barium site, which is ascribable to the lowering of the symmetry of the crystal structure (5).

In this study, we prepared the $Ba_{1-x}La_xPrO_3$ ($0 \leq x \leq 1.15$) solid solutions in which the oxidation state of praseodymium was reduced from the tetravalent state to the trivalent state with the lanthanum substitution for barium and have observed the change of the crystal structures and magnetic properties with the oxidation state of praseodymium. In addition, the $PrLu_{1-y}Mg_yO_3$($0 \leq y \leq 0.20$) solid solutions with the perovskite structure were prepared. In these solid solutions, the praseodymium ion is oxidized from the trivalent state to the tetravalent state with the magnesium substitution for lutetium. Through their magnetic susceptibility measurements, the differences in the magnetic properties of praseodymium ions between at the A-site and at the B-site of the perovskite structure were investigated.

EXPERIMENTAL

1. Sample Preparation

$Ba_{1-x}La_xPrO_3$ ($x = 0$, 0.025, 0.050, 0.075, 0.100, 0.125, and 0.150). La_2O_3, $BaCO_3$, and Pr_6O_{11} were used as starting materials. $BaCO_3$ and Pr_6O_{11} were heated at 200°C for several days to remove any moisture. La_2O_3 was heated at 900°C for 10 hours because of its high hygroscopicity. These reagents were weighed in correct metal composition ratios and ground intimately in an agate mortar.

0022-4596/99 $30.00

The mixtures were pressed into pellets and calcined in a flowing oxygen atmosphere at 1300°C for 24 hours. After cooling, the pellets were reground, repressed into pellets, and sintered once again at 1300°C for 24 hours under the same conditions to make the reaction complete. Since the $Ba_{1-x}La_xPrO_3$ loses a few oxygen atoms at high temperatures, the samples were annealed in an oxygen atmosphere at 1000°C for 48 hours.

$PrLu_{1-y}Mg_yO_3$ ($x = 0$, 0.025, 0.050, 0.075, 0.100, 0.125, 0.150, 0.175, and 0.200). Pr_6O_{11}, Lu_2O_3, and MgO were used as strating materials. The procedures to prepare these solid solutions were the same as those for $Ba_{1-x}La_xPrO_3$ solid solutions except for the heating procedure. The $PrLu_{1-y}Mg_yO_3$ solid solutions were heated in a flow of hydrogen atmosphere at 1350°C for 24 hours and then annealed in a flowing oxygen atmosphere at 600°C for 72 hours.

2. X-Ray Diffraction Analysis

X-ray powder diffraction profiles for the samples were measured using Rigaku RINT 2000 diffractometer with Cu$K\alpha$ radiation equipped with curved graphite monochromator. The data were collected by step scanning in the angle range $10° \le 2\theta \le 90°$ with increments of 0.04° and counting time of 5 sec per step. Indexing of the diffraction patterns and prediction of space groups for the $Ba_{1-x}La_xPrO_3$ and $PrLu_{1-y}Mg_yO_3$ solid solutions were performed by the computer program 'CELL.' The diffraction profiles were refined by the Rietveld analysis using the computer program 'RIETAN 94' and then the lattice parameters, atomic positions, bond lengths, and bond angles were determined (8).

3. Magnetic Susceptibility Measurements

The temperature dependence of magnetic susceptibilities was measured both with a Faraday-type torsion balance and a commercial SQUID magnetometer (Quantum Design, MPMS model).

The magnetic susceptibilities were measured in the temperature range between 4.2 and 273 K under the applied magnetic field of 4700, 6900, and 9000 G with the magnetic torsion balance. The equipment was calibrated with $Hg[Co(SCN)_4]$ as a standard. The temperature of the sample was measured by an Ag vs Au − 0.07 at.% Fe thermocouple in the range from 4.2 to 40 K and by an Au–Co vs Cu thermocouple in the range from 40 to 273 K. The magnetic susceptibilities for the samples were corrected for the quartz blank container.

The magnetic susceptibilities measurements with the SQUID magnetometer were carried out at 1000 G in the temperature range between 4.5 and 300 K. The temperature dependence of the magnetic susceptibilities was investigated under zero-field-cooled condition (ZFC) and field-cooled condition (FC). The magnetic hysteresis loops $M(H)$ were measured at 5 K in the magnetic field range $-50000\ \text{G} \le H \le 50000\ \text{G}$.

RESULTS AND DISCUSSION

1. Structural Properties

The X-ray diffraction patterns of the $Ba_{1-x}La_xPrO_3$ were indexed with the space group *Pnma*. They were formed in an orthorhombically distorted perovskite. The variation of lattice parameters for the $Ba_{1-x}La_xPrO_3$ solid solutions with the lanthanum concentration (x) is shown in Fig. 1. The lattice parameters increase with La^{3+} concentration in the range $x \le 0.075$. On the other hand, the lattice parameters are almost constant above $x = 0.075$. From this lattice parameter variation, it is considered that the single phase solid solutions were obtained in the range $x \le 0.075$. It is discussed that the increase of lattice parameters is mainly due to the results of the variation in ionic size of the *B*-site in the perovskite ABO_3. In the *A*-site, the average ionic radius decreases with increasing x value, which is caused by the substitution of the smaller La^{3+} for the Ba^{2+} site; i.e., the ionic radius of La^{3+} (the coordination number is 12 (C.N.XII)) is 1.36 Å and that of Ba^{2+} (C.N.XII) is 1.61 Å (9). At the same time, some Pr^{4+} ions are reduced to the trivalent state to preserve the charge neutrality in solids. The ionic radius of Pr^{3+} (C.N.VI) is 0.99 Å and that of Pr^{4+} is 0.85 Å (9). The increase of the average ionic size of the

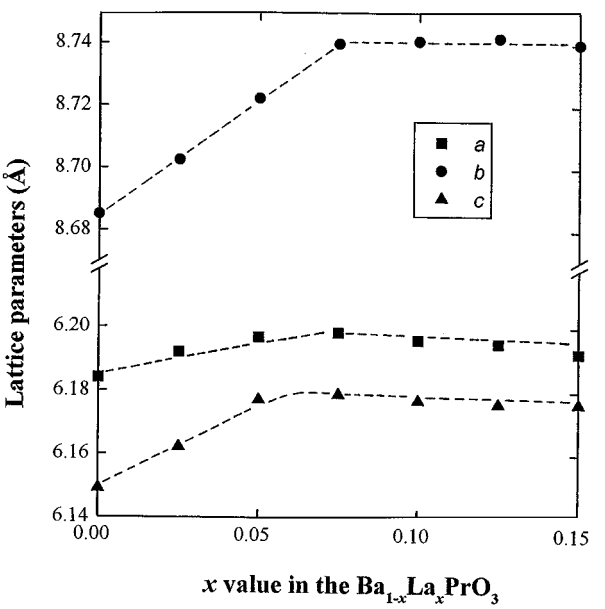

FIG. 1. Variation of lattice parameters for $Ba_{1-x}La_xPrO_3$ with La concentration (x value).

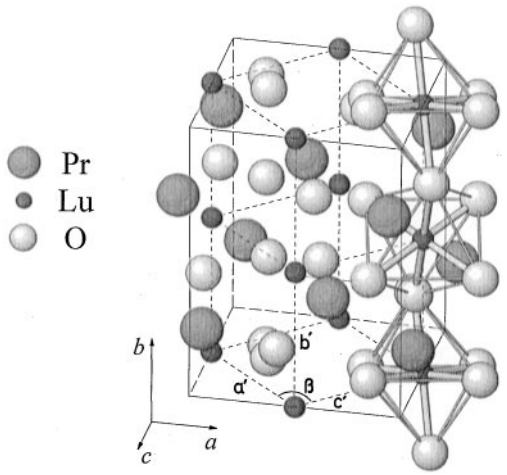

FIG. 2. Crystal structure of $PrLuO_3$.

B-site is found to significantly affect the cell size of the perovskite ABO_3.

Figure 2 shows the crystal structure of $PrLuO_3$ determined in this study. This $PrLuO_3$ is an orthorhombically distorted perovskite and its space group is *Pnma*, which is the same as the case of $Ba_{1-x}La_xPrO_3(0 \leq x \leq 0.075)$. The preparation of $PrLuO_3$ was not reported. Our study is the first preparation of $PrLuO_3$ and the first determination of its crystal structure. The observed, calculated, and difference profiles of the X-ray diffraction for $PrLuO_3$ are plotted in Fig. 3, and the results of the Rietveld analysis are listed in Table 1. The lattice parameters for the $PrLuO_3$ are $a = 5.9868(1)$ Å, $b = 8.3202(2)$ Å, and $c = 5.7604(1)$ Å. In the true crystallographic cell, there are four primitive perovskite unit cells (see Fig. 2). The perovskite pseudo-cubic cell parameters are $a' = c' = 4.1540(2)$ Å, $b' = 4.1601(1)$ Å, and $\beta = 92.21(1)^\circ$. The deviation from the ideal perovskite cubic cell is significantly large in the $PrLuO_3$.

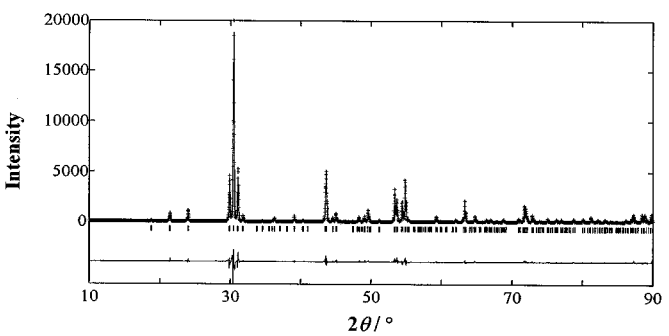

FIG. 3. Powder X-ray diffraction pattern fitting for $PrLuO_3$. The calculated and observed patterns are shown on the top solid line and dots. The vertical marks in the middle show positions calculated for Bragg reflections. The trace on the bottom is a plot of the difference between calculated and observed intensities.

TABLE 1
Atomic Positions, Bond Lengths (in Angstroms), and Bond Angles (in Degrees) for $PrLuO_3$

Atom	*x*	*y*	*z*	
		Atomic positions		
Pr	0.0546(8)	0.2500	−0.0149(12)	
Lu	0.5000	0.0000	0.0000	
O(1)	0.4373(87)	0.2500	0.1169(90)	
O(2)	0.3080(66)	0.0620(49)	0.6837(67)	
		Bond lengths		
Pr–O(1)	2.398(8) × 1	2.414(9) × 1	3.538(10) × 1	3.773(10) × 1
Pr–O(2)	2.361(8) × 2	2.786(9) × 2	2.954(9) × 2	3.885(10) × 2
	Lu–O(1)	2.218(8) × 2		
	Lu–O(2)	2.188(7) × 2	2.215(8) × 2	
		Bond angles		
	Lu–O(1)–Lu	139.3(5)	Lu–O(2)–Lu	141.3(5)

Note. $R_{wp} = 15.30\%$, $R_p = 11.37\%$. Definitions of *R*'s: $R_{wp} = 100 \times \{[\sum_w (I_{obs} - I_{calc})^2]/[\sum_w (I_{obs})^2]\}^{1/2}$; $R_p = 100 \times \sum |I_{obs} - I_{cacl}| / \sum I_{obs}$.

X-ray diffraction measurements for $PrLu_{1-y}Mg_yO_3$ solid solutions show that the orthorhombic perovskite phase is formed in the range of $y \leq 0.075$ and that the cubic (*C*-type) rare earth sesquioxide phase is formed in the range of $y \geq 0.20$. In the range between $0.075 < y < 0.20$, there exists a complex phase composed of the perovskite and the *C*-type rare earth sesquioxide. With the substitution of the Mg^{2+} for Lu^{3+} in the $PrMg_yLu_{1-y}O_3$ solid solutions, some of the Pr^{3+} ions are oxidized to the tetravalent state to preserve the charge neutrality in solids. The generation of smaller Pr^{4+} ions at the *A*-site of the ABO_3 no longer stabilize the perovskite-type structure for $y \geq 0.20$ and forms the *C*-type rare earth sesquioxide.

The variation of lattice parameters for the $PrLu_{1-y}Mg_yO_3$ solid solutions ($y \leq 0.075$) with the magnesium concentration (y) is shown in Fig. 4. They decrease with increasing magnesium concentration. Substituting the Mg^{2+} ion for the Lu^{3+} ion in the $PrLu_{1-y}Mg_yO_3$ and therefore oxidizing the Pr^{3+} ions to the tetravalent state result in the decrease of both the ionic sizes of the *A*-sites and the *B*-sites of the perovskite ABO_3. Considering the case of the lattice parameter change for $Ba_{1-x}La_xPrO_3$ solid solutions, it is concluded that the decrease of lattice parameters for $PrLu_{1-y}Mg_yO_3$ solid solutions is mainly due to the decrease of the average ionic size of the *B*-sites.

2. *Magnetic Properties*

The temperature dependence of magnetic susceptibilities for the $Ba_{1-x}La_xPrO_3$ solid solutions in the x range $0 \leq x \leq 0.075$ is shown in Fig. 5. All the samples show an

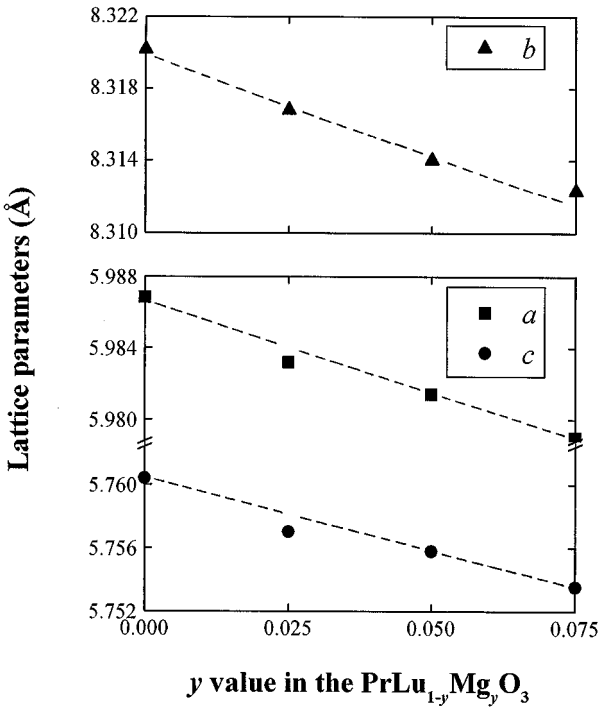

FIG. 4. Variation of lattice parameters for $PrLu_{1-y}Mg_yO_3$ with Mg concentration (y value).

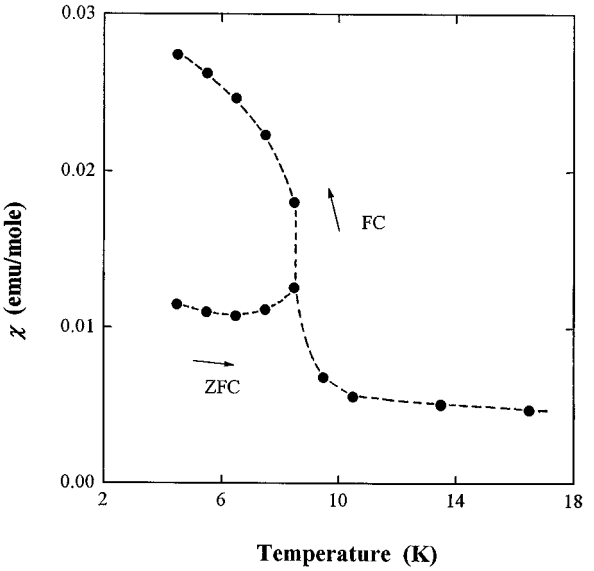

FIG. 6. Temperature dependence of magnetic susceptibility for $Ba_{0.925}La_{0.075}PrO_3$ at low tempertures measured with a SQUID magnetometer.

antiferromagnetic transition and the transition temperature decreases with increasing lanthanum concentration, indicating that the magnetic interactions between praseodymium ions are weakened by substituting the lanthanum ion for the barium ion. This weakening of magnetic ordering is considered to be caused by the structural change with lanthanum substitution. From the Rietveld analysis, the Pr–O–Pr bond angles in the $Ba_{0.925}La_{0.075}PrO_3$are 150.59° and 169.09°, which deviate from the ideal bond angle (=180°) for the antiferromagnetic superexchange interactions. These deviations are greater than those for $BaPrO_3$ (174.86° and 173.56°)(5). It should be also considered that the generation of the Pr^{3+} ion with the La^{3+} substitution for Ba^{2+} reduces the magnetic interaction between Pr^{4+} ions.

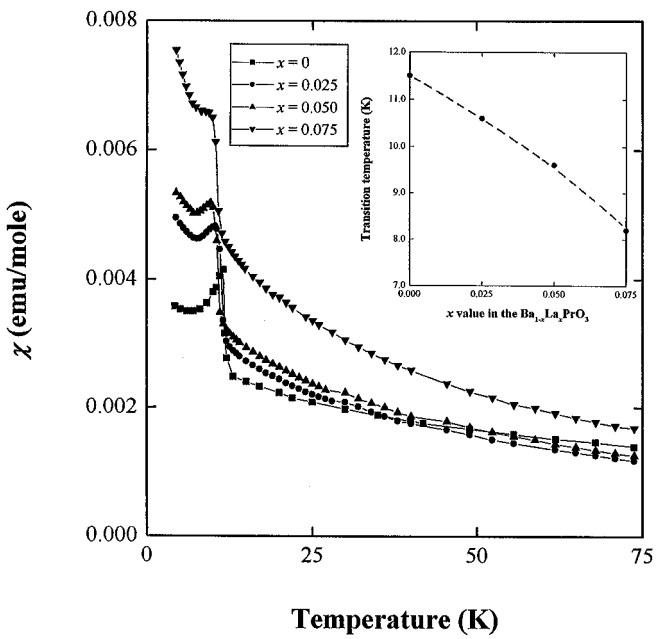

FIG. 5. Temperature dependence of magnetic susceptibilities for $Ba_{1-x}La_xPrO_3$ in the lower temperature range. Inset shows the variation of the magnetic transition temperature with x value.

The temperature dependence of magnetic susceptibility for the $Ba_{0.925}La_{0.075}PrO_3$ measured by the SQUID magnetometer is shown in Fig. 6. Below the transition temperature, the obvious divergence in the magnetic susceptibilities between ZFC and FC measurements was observed. It is presumed that such a behavior comes from a weak ferromagnetism associated with the antiferromagnetism caused by the canted spin of praseodymium. So, in order to clarify the magnetic behavior below the transition temperature, the magnetic hysteresis loop $M(H)$ under the magnetic field $-50{,}000\ \mathrm{G} \le H \le 50{,}000\ \mathrm{G}$ was measured at 5 K. However, the ferromagnetic component was not magnetized under this experimental applied field. Felner *et al.* reported that $BaPrO_3$ has a weak ferromagnetic moment below the transition temperature due to the Dzyaloshinsky–Moriya (D-M) interaction (4). The space groups of $Ba_{0.925}La_{0.075}PrO_3$ and $BaPrO_3$ are both *Pnma*, which allows the existence of the D-M interaction. Rosov *et al.* reported that the praseodymium ion in the $BaPrO_3$

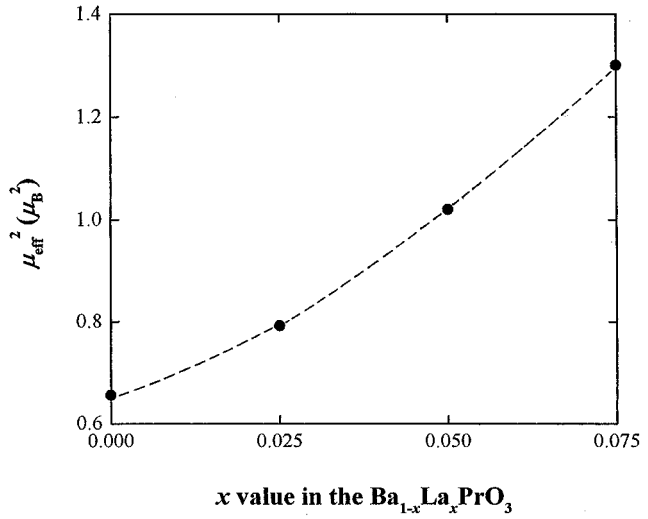

FIG. 7. Variation of the square of the effective magnetic moment of $Ba_{1-x}La_xPrO_3$ with La concentration (x value).

canted along its c-axis and the ferromagnetic moment was determined to be 0.35 μ_B from the high resolution powder neutron diffraction measurement (6).

Figure 7 shows the variation of the square of the effective magnetic moment of $Ba_{1-x}La_xPrO_3$ with lanthanum concentration. The effective magnetic moment increases with lanthanum concentration. This is due to the generation of the Pr^{3+} ion which has a larger magnetic moment than the Pr^{4+} ion. In $Ba_{1-x}La_xPrO_3$, there exist Pr^{3+} and Pr^{4+} ions and its ratio is $x:(1-x)$. If there is no magnetic interaction between Pr^{3+} and Pr^{4+} ions and their magnetic behavior follows the Curie–Weiss law; the square of the effective magnetic moment of $Ba_{1-x}La_xPrO_3$ is given by the following equation,

$$\mu^2 = x\mu^2(Pr^{3+}) + (1-x)\mu^2(Pr^{4+}), \qquad [1]$$

where $\mu(Pr^{3+})$ and $\mu(Pr^{4+})$ are the moments of Pr^{3+} ion and Pr^{4+} ion, respectively. By fitting Eq. [1] to the moments for $Ba_{1-x}La_xPrO_3$, the effective magnetic moments of Pr^{3+} and Pr^{4+} ions are obtained to be 2.61 and 0.81 μ_B, respectively. These values (especially the moment of Pr^{4+}) are smaller than the moments for the corresponding free ions (3.58 and 2.54 μ_B, respectively), indicating that the effect of the crystal field on the magnetic properties of the praseodymium ion at the B-site of the ABO_3 perovskite is large. Similar results have been obtained from the previous ESR measurements on a Pr^{4+} ion doped in $BaCeO_3$ (7).

To study the difference in the magnetic properties of praseodymium between at the A-site and at the B-site of the ABO_3 perovskite-type structure, the temperature dependence of magnetic susceptibilities for the $PrLu_{1-y}Mg_yO_3$ solid solutions ($0 \leq y \leq 0.075$) was measured in the temperature range between 4.2 and 300 K. These solid solutions show no magnetic ordering and were paramagnetic down to 4.2 K.

Figure 8 shows the variation of the square of the effective magnetic moment of $PrLu_{1-y}Mg_yO_3$ with magnesium concentration (y value). With substitution of the Mg^{2+} ion for the Lu^{3+} ion, some of the praseodymium ions are oxidized to the tetravalent state and the effective magnetic moment of the Pr^{4+} ion is smaller than that of the Pr^{3+} ion. Therefore, the effective magnetic moments of $PrLu_{1-y}Mg_yO_3$ solid solutions should decrease with increasing magnesium concentration, which is in accord with this experiment. In the $PrLu_{1-y}Mg_yO_3$, the ratio of Pr^{3+} and Pr^{4+} ions is $(1-y):y$. If we assume that there is no magnetic interactions between Pr^{3+} and Pr^{4+} ions, and that they follow the Curie–Weiss law, the effective magnetic moment of $PrLu_{1-y}Mg_yO_3$ is given by the following equation:

$$\mu^2 = (1-y)\,\mu^2(Pr^{3+}) + y\,\mu^2(Pr^{4+}). \qquad [2]$$

In a similar way as the case of $Ba_{1-x}La_xPrO_3$ solid solutions, by fitting Eq. [2] to the moments for $PrLu_{1-y}Mg_yO_3$, the effective magnetic moments of Pr^{3+} and Pr^{4+} ions in the $PrLu_{1-y}Mg_yO_3$ solid solutions are determined to be 3.28 and 2.24 μ_B, respectively. These are close to the moments for the corresponding free ions. Similar results are also reported for the $PrSc_{1-x}Mg_xO_3$ solid solutions, in which the effective magnetic moments of Pr^{3+} and Pr^{4+} are 3.54 and 2.53 μ_B, respectively (10). The praseodymium ion at

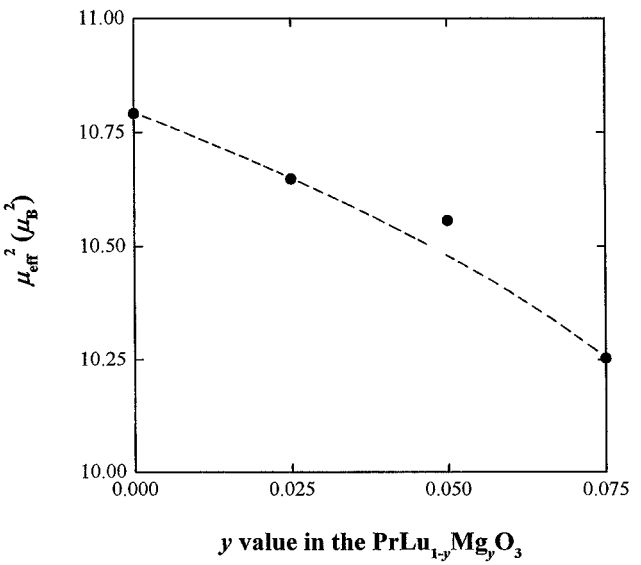

FIG. 8. Variation of the square of the effective magnetic moment of $PrLu_{1-y}Mg_yO_3$ with Mg concentration (y value).

the *A*-site of the ABO_3 perovskite is not much influenced by the crystal field.

From the results of effective magnetic moments of $Ba_{1-x}La_xPrO_3$ and $PrLu_{1-y}Mg_yO_3$, it has been cleared that the praseodymium ion situated at the *B*-site of the ABO_3 perovskite is influenced by the surrounding crystal field. This result is in accord with the difference in the Pr–O distances between in the $Ba_{1-x}La_xPrO_3$ solid solutions and in the $PrLu_{1-y}Mg_yO_3$ solid solutions. Our Rietveld analysis shows that in the former solid solutions, the Pr–O disance is 2.24 Å, while the Pr–O distance in the latter solid solutions is 2.99Å. The short distance between the metal ion and the oxygen ion has a stronger crystal field effect on the magnetic properties of the metal ion.

REFERENCES

1. N.E. Topp, "Chemistry of Rare-Earth Elements," Elsevier, Amsterdam, 1965.
2. Y. Hinatsu, *J. Solid State Chem.* **102,** 362 (1993).
3. J.B. Bulman, M.V. Kuric, R.P. Guertin, S. Foner, E.J. McNiff, Jr., G. Gao, J. O'Riely, J.E. Crow, P.P. Wise, and T. Yuen, *J. Appl. Phys.* **69,** 4874 (1991).
4. I. Felner, Y. Yeshurum, and G. Hilscher, *Phys. Rev. B* **46,** 9132 (1992).
5. M. Itoh and Y. Hinatsu, *J. Alloys Compounds* **264,** 119 (1998).
6. N. Rosov, *Phys. Rev. B* **45,** 982 (1992).
7. Y. Hinatsu and N. Edelstein, *J. Solid State Chem.* **112,** 53 (1994).
8. F. Izumi, *Nippon Kesshou Gakkaishi* **27,** 23 (1985).
9. R.D. Shannon, *Acta Crystallogr. Sect. A* **32,** 751 (1976).
10. Y. Takano and K. Sekizawa, *Kidorui* **30,** 266 (1997). [In Japanese]